Weak localization properties of the doped Z_2 topological insulator

Ken-Ichiro Imura, Yoshio Kuramoto, and Kentaro Nomura
Department of Physics, Tohoku University, Sendai 980-8578, Japan
(Received 11 May 2009; published 27 August 2009)

Localization properties of the doped Z_2 topological insulator are studied by weak localization theory. The disordered Kane-Mele model for graphene is taken as a prototype and analyzed with attention to effects of the topological mass term, intervalley scattering, and the Rashba spin-orbit interaction. The known tendency of graphene to antilocalize in the *absence* of intervalley scattering between K and K' points is naturally placed as the massless limit of the Kane-Mele model. The latter is shown to have a unitary behavior even in the absence of magnetic field due to the topological mass term. When intervalley scattering is introduced, the topological mass term leaves the system in the unitary class, whereas the ordinary mass term, which appears if A and B sublattices are inequivalent, turns the system to weak localization. The Rashba spin-orbit interaction in the *presence* of K-K' scattering drives the system to weak antilocalization in sharp contrast to the ideal graphene case.

DOI: 10.1103/PhysRevB.80.085119 PACS number(s): 72.10.−d, 72.15.Rn, 73.20.Fz

I. INTRODUCTION

The concept of Z_2 topological insulator was first introduced in a model for graphene,[1] in the presence of both intrinsic and extrinsic (Rashba) spin-orbit interactions (called hereafter, Kane-Mele model).[2,3] The origin of Z_2 symmetry lies naturally in the time-reversal invariance of the underlying spin-orbit interactions, i.e., in the existence of Kramers pairs. In the continuum limit, the intrinsic spin-orbit interaction is represented by a so-called topological mass term (of size Δ, opening a spin-orbit gap 2Δ), encoding quantized spin-Hall effect. The latter occurs when Fermi energy is in the gap and implies the existence of a pair of counterpropagating gapless states at the sample boundary with opposite spins, often dubbed as *helical* edge modes.[4] The idea of "Z_2" topological insulator stems from the observation that these helical edge modes are robust against weak perturbations, such as the extrinsic Rashba spin-orbit interaction (coupling strength: λ_R). Thus, nontrivial topological nature of a Z_2 topological insulator is often attributed to the existence of such edge modes, protected by Kramers degeneracy. This paper, on the contrary, highlights its *bulk* property. Since real materials always have disorder, we investigate its transport property *under doping* using the framework of standard weak localization (WL) theory.

Of course, the magnitude of spin-orbit interactions has always been questioned in graphene,[5–7] leading to search for Z_2 nature in a system of larger spin-orbit coupling.[4,8] The existence of helical edge modes was first experimentally shown in a two-dimensional (2D) HgTe/CdTe heterostructure.[8] Recall that in graphene two doubly degenerate Dirac cones appear at K and K' points in the first Brillouin zone,[1] in contrast to a single pair of Dirac cones appearing at the Γ point in HgTe/CdTe quantum well. The first estimate of Δ and λ_R in the original paper of Kane and Mele: $2\Delta \sim 2.4$ K and $\lambda_R/2 \sim 0.5$ mK for a typical strength of perpendicular electric field $E=50$ V/300 nm, provides a favorable condition for Z_2 nontrivial phase.[2] This estimate was later shown to be too optimistic (for the occurrence of Z_2 phase) due to the specific geometry of s and p orbitals in graphene. According to Ref. 5, the estimated value of Δ (λ_R) is much smaller (larger) than the original estimation of Ref. 2: $2\Delta \sim 0.01$ K and $\lambda_R/2 \sim 0.13$ K for the same electric field of $E=50$ V/300 nm. On the other hand, a recent first-principle calculation suggests that d orbitals play a dominant role in the gap opening at K and K' points.[9] As a result, the actual value of Δ might be somewhat intermediate between the previous estimates of Refs. 2 and 5–7, namely, $2\Delta \sim 0.28$ K and $\lambda_R/2 \sim 0.23$ K per V/nm. The concept of Z_2 topological insulator has also been extended to three space dimensions.[10–17]

Localization properties of the doped Kane-Mele Z_2 insulator have been studied numerically.[18,19] Reference 18 deduces a phase diagram in the (E,W) plane (E: energy and W: strength of disorder) in which a metallic domain appears in valence and conduction bands with a finite width in E. As disorder is increased, these two extended domains in both bands approach to each other, and eventually merge and disappear. A more subtle issue is the nature of the metallic state next to the Z_2 insulating phase. It has been claimed[18] that the system's Z_2 symmetry leads to an unconventional symmetry class. However, an extensive study on the critical exponents[19] has suggested that the weak antilocalization (AL) behavior of the doped Z_2 insulator belongs to the conventional symplectic symmetry class. This paper addresses the basic mechanism how doped Z_2 insulators acquire such unique localization properties. As a simple implementation of Z_2 topological insulator, we consider Kane-Mele model and in contrast to the numerical works of Refs. 18 and 19, we restrict our study to the limit of weak disorder. On the other hand, we pay much attention to the existence of *valleys* in graphene since localization properties are much influenced by the presence or absence of scattering across different valleys in the Brillouin zone. The later is determined by the range of the impurity potential.[20]

This paper is organized as follows. The Kane-Mele model is introduced in Sec. II. Then, we apply the standard diagrammatic approach to weak localization to the doped Kane-Mele model. In Sec. III we consider the case of vanishing Rashba silicon-on-insulator (SOI). Particular attention will be paid to different types of the mass term, (a) and (b), to-

TABLE I. Three story structure of the Kand-Mele Z_2 topological insulator, In addition to the real spin $\vec{s}$, there appear two types of pseudospins: $\vec{\sigma}$ representing A-B sublattices and $\vec{\tau}$ specifying the valley: K or K'. (*) if Fermi level is in the gap.

	Long-range scatterers (single valley)	Short-range scatterers (K-K' coupled by intervalley scattering)
(i) Ideal graphene (massless)	$H_1=\hbar v_F(p_x\sigma_x+p_y\sigma_y)$ single Dirac cone	$H_1=\hbar v_F(p_x\sigma_x\tau_z+p_y\sigma_y)$ opposite chiralities at K and K'
(ii) Mass terms: (a) topological → QSH insulator* (b) ionic → ordinary insulator*	$H_2=m\sigma_z$	(a) $H_2=-\Delta\sigma_z\tau_z s_z\equiv H_\Delta$ (b) $H_2=M\sigma_z\equiv H_M$
(iii) Rashba spin-orbit interaction →Z_2 topological insulator	$H_R=-\lambda_R(\sigma_x\tau_z s_y-\sigma_y s_x)$ mixes real spin ↑ and ↓ (spin rotational-symmetry broken)	

gether with the presence/absence of K-K' scattering. Here, we will focus on unitary behaviors, which appear as a consequence of a finite lifetime acquired by Cooperons. Breaking or preserved effective time-reversal symmetry (TRS) will be the main issue of this section. Section IV is devoted to study on the effects of Rashba spin-orbit interaction. In the final section, we will summarize our results and give interpretation to them in terms of the number of *active* species of effective spins.[21]

II. KANE-MELE MODEL

The Kane-Mele model is given a status as a prototype for various Z_2 topological insulator models. It was introduced as a model for graphene in the presence of spin-orbit interactions.[2] The model is first defined on the hexagonal lattice, in the framework of tight-binding approximation. The continuum limit is then taken in which the effective Hamiltonian becomes

$$H_{\mathrm{KM}} = H_1 + H_\Delta + H_R,$$

$$H_1 = \hbar v_F(p_x\sigma_x\tau_z + p_y\sigma_y),$$

$$H_\Delta = -\Delta\sigma_z\tau_z s_z,$$

$$H_R = -\frac{\lambda_R}{2}(\sigma_x\tau_z s_y - \sigma_y s_x), \tag{1}$$

where three Pauli's matrices, $\vec{\sigma}$, $\vec{\tau}$, and $\vec{s}$ operate in different spaces. Namely, $\vec{\sigma}$ acts on pseudospin specifying the A-B sublattices, $\vec{\tau}$ on the K-K' "valley spin," and $\vec{s}$ on the real spin. Throughout this paper, we assume that $\Delta>0$.[22]

A. Three story structures

The Kane-Mele model defined as Eq. (1) has the following three story structures (see Table I), corresponding to each term of Eq. (1): (i) graphene on its base, (ii) a topological mass term, encoding quantized spin-Hall (QSH) effect, and finally (iii) the Rashba spin-orbit interaction λ_R. Let us first look into the role of these three floors one by one.

1. Graphene and its localization properties

Graphene, an isolated single layer of graphite, has a band structure with two massless points (often referred to K and K') in the first Brillouin zone and in the vicinity of these points the low-energy effective Hamiltonian reduces to a Dirac-Weyl form.[1] This part of the Hamiltonian, i.e., H_1 in Eq. (1), comes from the standard nearest-neighbor-hopping term in the tight-binding approximation. Such ideal (massless) graphene shows weak antilocalization behavior,[23–25] when intervalley (K-K') scattering is irrelevant.[23] The absence or presence of K-K' scattering is determined by the range of scattering potential.[20] Short-(long-)range scatterers do (not) see the difference between A and B sites and also do (not) involve K-K' scattering. The weak localization behavior of graphene is indeed susceptible of the presence or absence of K-K' scattering.[23,26] In the absence of K-K' scattering, it is now established[27] that at one-loop order the graphene (a single Dirac cone) shows a weak antilocalization behavior, indicating that the system is symplectic.[28]

An interesting question is to what extent this antilocalization tendency continues against generalizations. Recent numerical analyses suggest that this antilocalization tendency actually continues to the strong-coupling regime,[24,25] due probably to some cancellation of higher order terms in the expansion of $\beta(g)$. Reference 24 argues that such cancellation of higher order terms is a consequence of a nontrivial spectral flow, associated with Z_2 Kramers symmetry, from which they coined the word, "Z_2 (topological) metal." It is also pointed out that unconventional behaviors of Z_2 metal can also be casted in terms of a topological term in the effective σ-model description.[29] In this paper, we achieve another generalization of Ref. 23 by reinterpreting the weak antilocalization property of graphene as the massless limit of a more general system, i.e., that of the Kane-Mele QSH insulator.

Let us go back to the explicit form of Eq. (1) and focus on its properties under time-reversal operation. The TRS plays an essential role in the discussion of symmetry classes in weak localization theory. In the absence of K-K' scattering, the two Dirac cones are decoupled dynamically, whereas TRS operation transforms K to K' and vice versa. In such cases, it is convenient to introduce the idea of "pseudo time-reversal symmetry" (PTRS) (Ref. 30) in which one pretends that $\vec{\sigma}$ represents a real spin so that pseudo-Kramers' pairs are formed in a single Dirac cone. Then PTRS transforms $\vec{p}$ to $-\vec{p}$ within a valley. Since $\vec{\tau}$ is invariant under PTRS by definition, H_1 is also invariant. Unlike the real spin, however,

the pseudospin should have single-valued eigenstates. This apparent difficulty is resolved in terms of the Berry phase[20] as discussed shortly toward the end of this section.

2. Topological mass and the quantized spin-Hall effect

In the second row of Table I shows the two Dirac cones at K and K' valleys of graphene acquire a gap (the total Hamiltonian becomes $H=H_1+H_2$) either in the presence of (a) imaginary hopping between second-nearest neighbors due to spin-orbit interaction[2] or (b) AB sublattice symmetry-breaking staggered chemical potential. In case (a), the so-called topological mass term H_Δ is generated, whereas (b) leads to a standard ionic mass term H_M.

First note that in case (a), the topological mass term $H_\Delta=-\Delta\sigma_z\tau_z s_z$ is time-reversal invariant. This stems from the fact that spin-orbit interaction preserves TRS. Second, note also that this is true only when we count both the (real) spin-up and spin-down sectors. Namely, if we pick up, say, only up-spin part, then the system breaks TRS, showing, e.g., a finite σ_{xy} $(=\pm e^2/h$, see below) even in the absence of magnetic field.[33] On the other hand, (b) a staggered chemical potential generates a mass term of the form: $H_M=M\sigma_z$, which has the same sign at K and K' points. The total Hamiltonian $H=H_1+H_M$ describes an ordinary insulator such as a monolayer of boron nitride.

Consideration on such different types of energy gap[33] naturally leads to the idea of "quantized" spin-Hall insulator.[2] In contrast to the ordinary ionic mass case (b), where the so-called parity anomaly cancels between the K and K' points and does not manifest itself,[32] the topological mass term (a) has an opposite sign at K and K' points[33] as well as for up and down spins, resulting in the quantized spin-Hall effect. There are actually two copies of quantum Hall states à la Ref. 33 under zero magnetic field, one with spin $\uparrow$ and $\sigma_{xy}^{\uparrow}=+e^2/h$, and the other with spin $\downarrow$ and $\sigma_{xy}^{\downarrow}=-e^2/h$.[2]

The existence of an energy gap is also suggested in experiments. Its magnitude is under debate in photoemission experiments.[34,35] In contrast to the theoretical prediction,[23,24,27] weak localization experiments on graphene[36–38] show also a unitary behavior. It is, therefore, natural to ask how the localization properties would be influenced by the presence of mass term. Absence of WL may be attributed to ripples.[39,40]

The type of mass term, given either by H_Δ or H_M, is a relevant factor in our discussion on localization properties (see later sections). If there is no K-K' scattering and two Dirac cones are decoupled, however, the system cannot see the difference between the two types of mass term. The behavior of the system is thus strongly dependent on the presence or absence of K-K' scattering. We will see in later sections, when K-K' scattering is switched on, the topological mass (b) leaves the system unitary, whereas the ordinary mass drives the system to orthogonal symmetry class. Our analysis will be summarized in the language of PTRS in the final section (see Table II) and should be applicable to two-dimensional Z_2 insulators in general.

3. Rashba spin-orbit interaction and Z_2 topological order

Let us finally consider the third row (iii) of Table I in which the total Hamiltonian becomes $H=H_1+H_2+H_R$. The Rashba term H_R turns out to be a relevant perturbation to the above symmetry properties. First, as for topological properties of the undoped phase, the quantized spin-Hall effect is not robust but replaced by a Z_2 topological order.[3]

As for weak localization properties of the doped phase, the Rashba term H_R, fixing the relative angle between s_z and the real space coordinates, changes the symmetry class. We will see in Sec. IV that the Rashba spin-orbit interaction turns the system from unitary to orthogonal in the absence of K-K' scattering, whereas in the presence of K-K' scattering, the system turns from unitary to symplectic with weak antilocalization behavior. In the present "poor man's" analysis, we can identify the scattering channel that separates these different symmetry classes. The two weak antilocalization phases, one in the ideal (massless) graphene limit (single Dirac cone, unconventional) and the other associated with a Z_2 topological insulator, evolve from each other via either orthogonal or unitary behavior, activated by the Rashba term together with K-K' scattering or the topological mass, respectively.

Let us emphasize that the weak antilocalization behavior of graphene occurs in the phase diagram of no K-K' scattering, whereas the weak antilocalization of Z_2 topological insulator occurs *due to* K-K' scattering. In the previous numerical analysis,[18,19] this important fact has not been noticed because the disorder in the real-space model always involved the effective intervalley scattering.

B. Construction of eigenstates

To construct eigenstates explicitly, we first consider the simplest nontrivial case with vanishing Rashba interaction and allow only long-range scatterers (LRS). Since $\lambda_R=0$, real spin-up and spin-down sectors become decoupled. In terms of the Hamiltonian, $H=H_1+H_2$ is diagonal in real spin $\vec{s}$ space as well as in τ-spin space. We can, therefore, consider separately $\tau_z=1$ (K valley) and $\tau_z=-1$ (K' valley). Taking $\hbar=v_F=1$ for simplicity, one may rewrite the Hamiltonian in the K valley, $H=H_1+H_\Delta$ (with $\tau_z=1$ and $s_z=1$), in the following simple form:

$$H=\vec{p}\cdot\vec{\sigma} \tag{2}$$

by introducing a fictitious three-dimensional momentum $\vec{p}=(p_x,p_y,-\Delta)$. As for $H=H_1+H_M$, one has simply to replace it with $\vec{p}=(p_x,p_y,M)$.

The Hamiltonian can then be diagonalized by choosing a proper quantization axis of the pseudospin, in analogy to the SU(2) spin case. One must take into account here that the $\vec{\sigma}$ represents only a pseudospin as it is derived from the sublattice degree of freedom. Correspondingly, the momentum $\vec{p}$, specifying the quantization axis for $\vec{\sigma}$ is *single valued*. Taking this single valuedness also into account, one may denote the eigenvalues and the eigenvectors of $H=H_1+H_2$ as

$$H|\vec{p}\pm\rangle=\pm|\vec{p}||\vec{p}\pm\rangle=\pm\sqrt{p_x^2+p_y^2+\Delta^2}|\vec{p}\pm\rangle,$$

$$|\vec{p}+\rangle = \begin{pmatrix} \cos\frac{\theta}{2} \\ e^{i\phi}\sin\frac{\theta}{2} \end{pmatrix}, |\vec{p}-\rangle = \begin{pmatrix} \sin\frac{\theta}{2} \\ -e^{i\phi}\cos\frac{\theta}{2} \end{pmatrix}, \quad (3)$$

where θ and ϕ are polar angles satisfying

$$\cos\theta = \frac{-\Delta}{\sqrt{p_x^2+p_y^2+\Delta^2}}, \quad \cos\phi = \frac{p_x}{\sqrt{p_x^2+p_y^2}}. \quad (4)$$

Here $|\vec{p}\pm\rangle$ corresponds to the upper-(lower-)band eigenvector. In the course of an adiabatic evolution of $|\vec{p}(t)\pm\rangle$ around the origin of $\vec{p}$, however, a Berry phase π enters per winding.[41] This situation keeps consistency with the double-valued SU(2) eigenstates of a real spin.[42]

In the following we will focus on the upper (conduction) band with $E=|\vec{p}|\geq\Delta$. One can also write down the eigenstates in the K' valley using the same parametrization. Because $\tau_z=-1$ in the K' valley, the conduction band has eigenfunctions of the form $|\vec{p}-\rangle$ in Eq. (3) with ϕ replaced by $-\phi$. We also introduce the notation, α, α', β, etc., to specify the momentum $\vec{p}$, in order to keep the consistency in notation with Ref. 23. For example, we will use notations such as,

$$|K\alpha\rangle = |\vec{p}+\rangle = \begin{pmatrix} \cos\frac{\theta_\alpha}{2} \\ e^{i\phi_\alpha}\sin\frac{\theta_\alpha}{2} \end{pmatrix}, \quad (5)$$

$$|K'\alpha\rangle = \begin{pmatrix} e^{i\phi_\alpha}\sin\frac{\theta_\alpha}{2} \\ -\cos\frac{\theta_\alpha}{2} \end{pmatrix}. \quad (6)$$

As long as the Rashba term is absent, one can safely fix $\vec{s}$, say, to be $\uparrow$. Then we do not explicitly consider the real spin until Sec. IV.

III. WEAK LOCALIZATION PROPERTY: UNITARY CASES

WL phenomena have been known since three decades.[43] Scaling to metal (weak antilocalization) was shown to be possible due to scattering by spin-orbit interaction.[44] Absence of WL (unitary behavior) is, on the other hand, attributed to explicit breaking of TRS. This paper shows that in systems of graphene, a zoo of such different localization behaviors appears under the same Hamiltonian, simply by activating or inactivating effective spin degrees of freedom (Fig. 1). Graphene thus provides a contemporary aspect to the conventional WL theory framework.

We apply standard diagrammatic techniques for weak localization to the doped Kane-Mele model. In real systems, such as a graphene sheet, doping can be easily done by simply applying a gate voltage. Suppose that our Fermi level is in the conduction band so that the system is metallic in the clean limit. We then introduce weak disorder by taking into account scattering by impurities. To characterize our two-dimensional system of size L^2, we focus on its longitudinal conductivity $\sigma_{xx}=g(L)$. Weak localization refers to $1/g$ correction to the so-called scaling function,

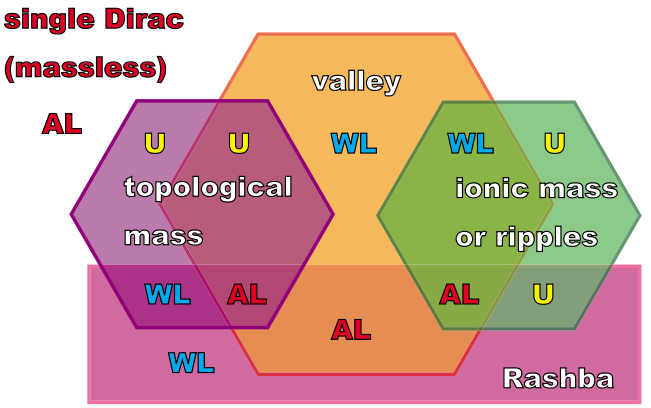

FIG. 1. (Color online) Weak localization phase diagram of the doped Kane-Mele model in the presence of potential scatterers. Relation to other graphene-based models with different types of the mass or ripples is taken into account. WL, AL, and U refer to weak localization (orthogonal class), weak antilocalization (symplectic class) and absence of WL (unitary class), respectively.

$$\beta(g) = \frac{d\log g}{d\log L} = D - 2 - \frac{c_1}{g} + \cdots, \quad (7)$$

where $\beta(g)\to 0$ $(g\to\infty)$ in two spatial dimensions $(D=2)$. $1/g$ correction to $\beta(g)$ leads to logarithmic corrections to conductivity. Thus, the sign of $1/g$ correction in Eq. (7), i.e., the sign of c_1 determines system's weak localization property: (i) $c_1>0$: WL (orthogonal), (ii) $c_1=0$: absence of WL peak in magneto-resistance data (unitary), and (iii) $c_1<0$ (symplectic). Symmetry classes (orthogonal, unitary, and symplectic) are due to the classification of corresponding random matrices.[28] Such logarithmic corrections to conductivity can be calculated using diagram techniques based on Kubo formula.[45] Diagrams contributing to a weak localization correction are particle-particle-type ladders or sometimes also called a "Cooperon." In contrast to the particle-hole-type diagrams, which *always* show a "diffusion-type" $1/q^2$ singularity, whether Cooperon diagrams are susceptible of such $1/q^2$ singularity is a more subtle issue related to time-reversal symmetry of the system.[43]

In this section, we first switch *off* Rashba spin-orbit interaction and study whether different types of mass term lead to the absence of WL peak (unitary behavior). We consider only scalar potential scatterers in contrast to Ref. 44. Instead, we distinguish impurities of different potential range and classify them into two categories, depending on whether they involve intervalley scattering or not. Charged Coulomb impurities are long-ranged, and cannot see the lattice structure. they do not couple K and K', either. On the contrary, scattering due, e.g., to defects has a potential range comparable to the lattice constant, and does connect different valleys.

A. Long-range scatterers

Long-range scatterers involve only intravalley scattering. One can, therefore, safely focus on, say, the K-valley. Such

scatterers do not distinguish between A- and B-sublattices, either, i.e., the impurity vertex is also unity in the A-B sublattice space. The matrix element associated with long-range scatterers is, therefore, proportional to

$$\langle K\beta|1|K\alpha\rangle = \cos^2\frac{\theta}{2} + e^{i(\phi_\alpha-\phi_\beta)}\sin^2\frac{\theta}{2}, \tag{8}$$

where we assumed elastic scattering ($\theta_\alpha=\theta_\beta=\theta$). Note that here we pick up only the spin part of the matrix element and $|K\alpha\rangle$ represents only the spinor part of the electron wave function. In order to find the full matrix element between different momentum eigenstates, Eq. (8) should be appended by a spatial part that requires the momentum conservation. The phase factor in Eq. (8) is analogous to the Berry phase, which has already appeared in Ref. 42, in the graphene limit ($\theta\to\pi/2$). The Berry phase, in the presence of a mass term, is not generally π in contrast to the massless limit. Note also that Eq. (8) involves an imaginary part that indeed turns the system from weak localization to weak antilocalization. In the present case, its complex nature does not come from the scattering potential but from the property of wave function.

From the self-energy diagram, we define the scattering time τ_L as,

$$\frac{1}{\tau_L} = 2\pi\nu(E)n_L u_L^2\langle|\langle K\beta|1|K\alpha\rangle|^2\rangle = \eta_L\left(\cos^4\frac{\theta}{2} + \sin^4\frac{\theta}{2}\right), \tag{9}$$

where n_L, u_L, and $\nu(E)$ are, respectively, the impurity density, the strength of impurity scattering potential, and the density of states at the given energy E. They combine to give $\eta_L = 2\pi\nu(E)n_L u_L^2$ and $\langle\cdots\rangle$ represents the angular part of impurity average.

The transport relaxation time τ_{tr} involves the $\cos(\phi_\alpha - \phi_\beta)$ term as

$$\begin{aligned}\frac{1}{\tau_{tr}} &= \eta_L\langle|\langle K\beta|1|K\alpha\rangle|^2[1-\cos(\phi_\alpha-\phi_\beta)]\rangle \\ &= \eta_L\left[\cos^4\frac{\theta}{2} + \sin^4\frac{\theta}{2} - \frac{\sin^2\theta}{4}\right],\end{aligned} \tag{10}$$

where we have used $\langle\cos(\phi_\alpha-\phi_\beta)\rangle=0$ and $\langle\cos^2(\phi_\alpha-\phi_\beta)\rangle = 1/2$. Usually, the factor $1-\cos(\phi_\alpha-\phi_\beta)$ in the first line of Eq. (10) is inactive for δ function like (s-wave) scatterers. Here, the matrix (Dirac) nature of the Hamiltonian induces a cosine term that corresponds to vertex correction in diagrammatic language.

The bare vertex function γ has also ϕ dependence

$$\begin{aligned}\gamma &= \eta_L\left[\cos^4\frac{\theta}{2} + e^{i(\phi_\alpha-\phi_\beta)}\frac{\sin^2\theta}{2} + e^{2i(\phi_\alpha-\phi_\beta)}\sin^4\frac{\theta}{2}\right] \\ &= \gamma^{(0)} + \gamma^{(1)}e^{i(\phi_\alpha-\phi_\beta)} + \gamma^{(2)}e^{2i(\phi_\alpha-\phi_\beta)}.\end{aligned} \tag{11}$$

In the second line, we classify terms according to their relative angular momentum, i.e., different ϕ dependence: $e^{il(\phi_\alpha-\phi_\beta)}$, where $l=0,1,2$. This expansion helps to solve the Bethe-Salpeter equation,

$$\Gamma_{\alpha\beta} = \gamma_{\alpha\beta} + \gamma_{\alpha\mu}\Pi_\mu\Gamma_{\mu\beta}. \tag{12}$$

To find the solution of Eq. (12), we expand also Γ into different angular momentum components,

$$\Gamma_{\alpha\beta} = \Gamma^{(0)} + \Gamma^{(1)}e^{i(\phi_\alpha-\phi_\beta)} + \Gamma^{(2)}e^{2i(\phi_\alpha-\phi_\beta)}, \tag{13}$$

and integrate over ϕ_μ, i.e., over the intermediate angle dependence in Bethe-Salpeter equation. Notice also that $\Pi \simeq \tau_L(1-\tau_L Dq^2)$, with D being the diffusion constant: $D = v_F^2\tau_L/2$, one finds, at the same order of precision,

$$[1-\gamma^{(l)}\tau_L(1-\tau_L Dq^2)]\Gamma^{(l)} = \gamma^{(l)}. \tag{14}$$

The crucial issue is the cancellation (or not) of the leading order (~ 1) term in the coefficient of $\Gamma^{(l)}$. In the graphene limit ($\theta=\pi/2$), $\Gamma^{(1)}$ becomes $\sim 1/q^2$ singular driving the system to weak antilocalization. At the bottom of conduction band, on the other hand, $\Gamma^{(0)}$ becomes more important and toward the limit $\theta\to 0$ (though the model becomes ill defined in this limit), it tends to show $\sim 1/q^2$ singularity, leading the system to weak localization. Away from these limits, the system shows a unitary behavior, i.e., all the three Cooperons acquire a finite lifetime.

Here, let us recall that the weak localization refers to a logarithmic correction to the longitudinal conductivity σ_{xx}, of the form

$$\Delta\sigma_{xx} \sim \mp A\log\frac{L}{\bar{l}} \tag{15}$$

(L: size of the system, $\bar{l}$: mean-free path, and A: constant of order e^2/h). In front of the logarithmic term, $-$ sign should be chosen for the weak localization case. Whereas, in the case of weak antilocalization, this overall sign in front of the logarithmic divergence is positive (the correction tends to increase the conductivity). In the unitary case we mentioned above, the logarithmic divergence of Eq. (15) as $L\to\infty$ is cut off by the longest lifetime of a Cooperon. And in that sense, the behavior of the system is driven by the Cooperon of the longest lifetime. This situation is analogous to the case of spin-dependent scattering studied in Ref. 44. In order to quantify such unitary behaviors, we define the lifetime $\tau^{(l)}$ of a Cooperon, $\Gamma^{(l)}$ such that

$$\Gamma^{(l)} = \frac{1}{\tau_L^2(Dq^2 + 1/\tau^{(l)})}, \tag{16}$$

where all $\tau^{(l)}$'s are written in terms of a single parameter $\tan\theta/2$

$$\begin{aligned}\frac{\tau_L}{\tau^{(0)}} &= \tan^4\frac{\theta}{2}, \\ \frac{\tau_L}{\tau^{(1)}} &= \frac{1}{2}\left(\frac{1}{\tan(\theta/2)} - \tan\frac{\theta}{2}\right)^2, \\ \frac{\tau_L}{\tau^{(2)}} &= \frac{1}{\tan^4(\theta/2)}.\end{aligned} \tag{17}$$

Since we have $\tan(\theta/2)\leq 1$, there is no chance for Γ_2 to dominate. The parameter θ is transformed to energy E

$=\Delta/\cos\theta$. As E increases from $E=\Delta$, which means that θ increases from $\theta=0$, a crossover occurs at "universal" value,

$$\theta=\theta_c=2\arctan\frac{1}{\sqrt{2}}=1.23\cdots. \tag{18}$$

When $\theta_c<\theta<\pi/2$, $\Gamma^{(1)}$ (weak antilocalization) becomes dominant, leading to a *positive* logarithmic correction to the longitudinal conductivity of the form of Eq. (15) with the + sign but L replaced by $\tau^{(1)}$. When $\theta<\theta_c$, $\Gamma^{(0)}$ (weak localization) is dominant and the correction to σ_{xx} is given by Eq. (15) with the − sign. In terms of E, the crossover occurs at $E=E_c=3\Delta$ and at this point the logarithmic correction changes its sign. This crossover behavior is illustrated in Fig. 1, where we consider $\lambda_R=0$ for the moment.

Since long-range scatterers do not involve K-K' scattering and two Dirac cones are decoupled, the system cannot see the difference between the two types of mass terms. Thus for both types of mass terms, we found predominantly a unitary behavior. Cooperons acquire a finite lifetime, which plays the role of cutting off the logarithmic correction, Eq. (15). Typically, there is no $1/g$ correction to the $\beta(g)$ function in the $L\to\infty$ limit. However, one can still see a crossover from antilocalization tendency to weak localization regime, as far as the longest lifetime of a Cooperon is much larger than the system size L. When Fermi level is far above the gap, the electron does not feel very much that there is a gap, i.e., he has a tendency to behave as if he were a massless Dirac fermion (weak antilocalization behavior in the graphene limit, $E\to\infty$). As the Fermi level approaches the bottom of the band, the electron starts to feel the gap and when he is close, he even forgets about that he is actually a "relativistic fermion" and starts to behave (say, $E<3\Delta$) as if he were a nonrelativistic electron, showing the weak localization behavior.

B. Short-range scatterers with K-K' scattering

Short-range scatterers couple different valleys, i.e., K and K'. One may, therefore, possibly see the difference between two different types of masses; ordinary and topological. The scattering matrix elements involve also a projection operator in the AB sublattice space, i.e.,

$$\mathcal{P}_A=\begin{pmatrix}1&0\\0&0\end{pmatrix},\quad \mathcal{P}_B=\begin{pmatrix}0&0\\0&1\end{pmatrix}. \tag{19}$$

Matrix elements of such projection operators in the K valley are

$$\langle K\beta|\mathcal{P}_A|K\alpha\rangle=\cos^2\frac{\theta}{2},$$

$$\langle K\beta|\mathcal{P}_B|K\alpha\rangle=e^{i(\phi_\alpha-\phi_\beta)}\sin^2\frac{\theta}{2}. \tag{20}$$

Matrix elements of such projection operators involving K' valley depends, on the contrary, on the type of mass.

1. Topological mass case

Let us first consider the case of Kane-Mele quantized spin-Hall insulator, for which the conduction-band eigenkets are given by Eqs. (5) and (6). Since we are concerned about K-K' scattering, let us first consider the intervalley scattering matrix elements,

$$\langle K'\beta|\mathcal{P}_A\tau_-|K\alpha\rangle=e^{-i\phi_\beta}\sin\frac{\theta}{2}\cos\frac{\theta}{2},$$

$$\langle K\beta'|\mathcal{P}_A\tau_+|K'\alpha'\rangle=e^{i\phi_{\alpha'}}\sin\frac{\theta}{2}\cos\frac{\theta}{2},$$

$$\langle K'\beta|\mathcal{P}_B\tau_-|K\alpha\rangle=-e^{i\phi_\beta}\sin\frac{\theta}{2}\cos\frac{\theta}{2},$$

$$\langle K\beta'|\mathcal{P}_B\tau_+|K'\alpha'\rangle=-e^{-i\phi_{\alpha'}}\sin\frac{\theta}{2}\cos\frac{\theta}{2}, \tag{21}$$

where $\tau_\pm=(\tau_x\mp i\tau_y)/2$ are "spin-flip" operators associated with the valley-spin (K-K'). Their contribution to scattering time is, e.g.,

$$2\pi\nu(E)n_Au_A^2|\langle K'\beta|\mathcal{P}_A\tau_-|K\alpha\rangle|^2 + 2\pi\nu(E)n_Bu_B^2|\langle K'\beta|\mathcal{P}_B\tau_-|K\alpha\rangle|^2=2\gamma_S\sin^2\frac{\theta}{2}\cos^2\frac{\theta}{2}, \tag{22}$$

where we have defined

$$\eta_S=2\pi\nu(E)\frac{n_Au_A^2+n_Bu_B^2}{2}. \tag{23}$$

$n_{A,B}$ and $u_{A,B}$ are, respectively, the impurity density and the typical strength of scattering potential at the A (B) sites. In order to obtain the full expression for scattering time, one has to consider also the contributions from intravalley scattering, such as

$$2\pi\nu(n_Au_A^2|\langle K\beta|\mathcal{P}_A|K\alpha\rangle|^2+n_Bu_B^2|\langle K\beta|\mathcal{P}_B|K\alpha\rangle|^2) =2\pi\nu\left(n_Au_A^2\cos^4\frac{\theta}{2}+n_Bu_B^2\sin^4\frac{\theta}{2}\right). \tag{24}$$

Here, we assumed that the strength of intervalley scattering is the same as intravalley scattering but this simplification is irrelevant to our conclusions. The scattering time in the K valley reads

$$\frac{1}{\tau_K}=2\pi\nu n_Au_A^2(|\langle K\beta|\mathcal{P}_A|K\alpha\rangle|^2+|\langle K'\beta|\mathcal{P}_A\tau_-|K\alpha\rangle|^2) + 2\pi\nu n_Bu_B^2(|\langle K\beta|\mathcal{P}_B|K\alpha\rangle|^2+|\langle K'\beta|\mathcal{P}_B\tau_-|K\alpha\rangle|^2) \tag{25}$$

and one finds a similar expression for $\tau_{K'}$. One can verify, using Eqs. (22) and (24) that as far as $n_Au_A^2=n_Bu_B^2\equiv n_Su_S^2$, one finds

$$1/\tau_K=1/\tau_{K'}=\eta_S\equiv 1/\tau_S. \tag{26}$$

For short-range scatterers we consider here the transport relaxation time is identical to τ_S since the projection in the AB sublattice space leaves no cross term, i.e., ϕ-dependent term;

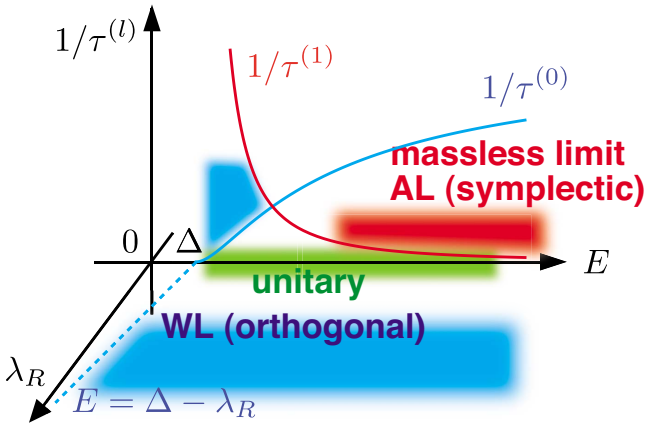

FIG. 2. (Color online) Weak localization properties for LRS without K-K' scattering. The ordinate shows crossover from WAL to WL tendency ($\lambda_R=0$, as E is decreased from the graphene limit toward the bottom of the band). Crossover from unitary to orthogonal symmetry class ($\lambda_R\neq 0$).

typically, $\sim\cos(\phi_\alpha-\phi_\beta)$, in the expression for $1/\tau_K$ and $1/\tau_{K'}$.

As for particle-particle ladders, the momentum conservation naturally leads us to classify them into KK, KK'-mixed, and $K'K'$ sectors. They correspond in the notation of Ref. 23, respectively, to $J=2$, 0, and -2 sectors. $J=j_\alpha+j_{\alpha'}=j_\beta+j_{\beta'}$ is conserved, where $j_\alpha=\pm 1$ if α occurs in the K (K') valley since $\vec{K}$-$\vec{K}'$ is only half of a reciprocal-lattice vector.

In the graphene limit,[23] the KK'-mixed sector is most divergent. In the $J=0$ sector, two types of Cooperon diagrams are possible (see Fig. 2). Both of them have two K electron and two K' electron lines but they appear either in the "cis" or "trans" arrangement (in the terminology of organic chemistry). Naturally, γ_c (γ_t) refers to cis (trans) and the same rule applies to $\Gamma_{c,t}$. The key issue here is that as a result of projection $\mathcal{P}_{A,B}$ and K-K' scattering, γ_t acquires an additional minus sign

$$\begin{aligned}\gamma_c &= 2\pi\nu n_A u_A^2\langle K\beta|\mathcal{P}_A|K\alpha\rangle\langle K\beta'|\mathcal{P}_A|K\alpha'\rangle \\ &\quad + 2\pi\nu n_B u_B^2\langle K'\beta|\mathcal{P}_B|K'\alpha\rangle\langle K'\beta'|\mathcal{P}_B|K'\alpha'\rangle \\ &= e^{i(\phi_\alpha-\phi_\beta)}\eta_S\frac{\sin^2\theta}{2}\equiv\gamma_c^{(1)}e^{i(\phi_\alpha-\phi_\beta)},\gamma_t \\ &= 2\pi\nu n_A u_A^2\langle K'\beta|\mathcal{P}_A\tau_-|K\alpha\rangle\langle K\beta'|\mathcal{P}_A\tau_+|K'\alpha'\rangle \\ &\quad + 2\pi\nu n_B u_B^2\langle K'\beta|\mathcal{P}_B\tau_-|K\alpha\rangle\langle K\beta'|\mathcal{P}_B\tau_+|K'\alpha'\rangle \\ &= -e^{i(\phi_\alpha-\phi_\beta)}\eta_S\frac{\sin^2\theta}{2}\equiv\gamma_t^{(1)}e^{i(\phi_\alpha-\phi_\beta)}(=-\gamma_c)\end{aligned} \tag{27}$$

cancelling with the Berry phase. Note also that as for ϕ dependence both γ_c and γ_t have only the $l=1$ component. Equation (27) is a simple consequence of the matrix elements in Eq. (21). Recall also that $\phi_\alpha-\phi_{\alpha'}=\pi$ since $k_\alpha+k_{\alpha'}=k_\beta+k_{\beta'}=q\simeq 0$.

In order to calculate the correction to conductivity, we set $\beta=\alpha'$, meaning $k_\alpha+k_\beta=q\simeq 0$, therefore, $\phi_\alpha-\phi_\beta=\pi$. The Bethe-Salpeter equation becomes two coupled equations

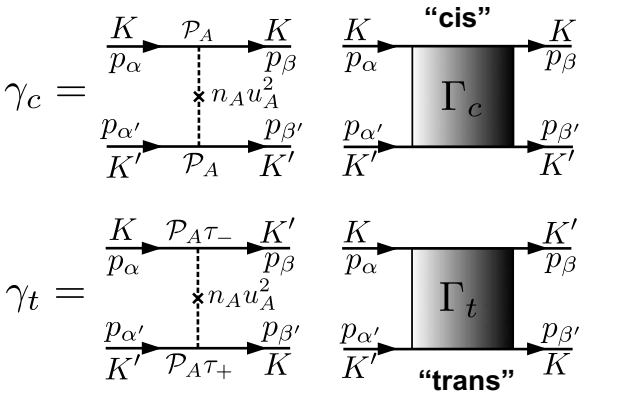

FIG. 3. Particle-particle ladders. Bare and dressed Cooperons. Relevant diagrams in the KK' sector. cis and trans refers to specific configurations of the valleys: K and K'.

$$\begin{pmatrix}\Gamma_c\\ \Gamma_t\end{pmatrix}_{\alpha\beta}=\begin{pmatrix}\gamma_c\\ \gamma_t\end{pmatrix}_{\alpha\beta}+\begin{pmatrix}\gamma_c & \gamma_t\\ \gamma_t & \gamma_c\end{pmatrix}_{\alpha\mu}\Pi_\mu\begin{pmatrix}\Gamma_c\\ \Gamma_t\end{pmatrix}_{\mu\beta}. \tag{28}$$

Indeed, both Γ_c and Γ_t contribute to the $1/q^2$ singularity. After diagonalization, one finds

$$\Gamma_c+\Gamma_t=0,$$

$$[1-(\gamma_c^{(1)}-\gamma_t^{(1)})\Pi_S](\Gamma_c-\Gamma_t)=\gamma_c-\gamma_t, \tag{29}$$

where $\Pi_S\simeq\tau_S(1-\tau_S Dq^2)$. The cancellation of the leading order (~ 1) term is incomplete, giving a finite lifetime $\tau_{KK'}$ to the Cooperon

$$\Gamma_t=\frac{-e^{i(\phi_\alpha-\phi_\beta)}}{2\tau_S^2(Dq^2+1/\tau_{KK'})}. \tag{30}$$

The lifetime $\tau_{KK'}$ behaves, as a function of E, like

$$\frac{\tau_S}{\tau_{KK'}}=\cot^2\theta=\frac{\Delta^2}{E^2-\Delta^2}. \tag{31}$$

Clearly, this KK' ($J=0$) Cooperon mode shows $1/q^2$ singularity only at the $E\to\infty$ limit.[23] Decreasing energy toward the bottom of the band, another KK ($J=2$) mode becomes important. The lifetime of the latter Cooperon (KK mode) behaves, as a function of E, like

$$\frac{\tau_S}{\tau_{KK}}=\frac{E^2-\Delta^2}{E^2+\Delta^2}. \tag{32}$$

Thus, except at $E=\Delta$ and $E\to\infty$, all the Cooperons having a finite lifetime, the system shows a unitary behavior with no $1/g$ correction in the $L\to\infty$ limit (see Fig. 3).

One may find this contradictory to the fact that the topological mass term $-\Delta\sigma_z\tau_z s_z$ does preserve TRS. To clarify this point, first note that the entire Hamiltonian (1) is time-reversal invariant and that this comes from the fact that spin-orbit interaction preserves TRS. Second, note also that this is true *only when we count both the (real) spin-up and spin-down sectors* and that if we pick up, say, only up-spin part, then the system showing, e.g., a finite σ_{xy} ($=\pm e^2/h$) even in the absence of magnetic field,[33] clearly breaks TRS. In the absence Rashba spin-orbit interaction, spin-up and spin-

down sectors are actually decoupled, indicating that the system belongs to the unitary class.[46]

2. Ordinary mass case

In the case of ordinary mass, one has to replace $|K'\alpha\rangle$ in Eq. (6) with

$$|K'\alpha\rangle = \begin{pmatrix} e^{i\phi_\alpha}\cos\frac{\theta_\alpha}{2} \\ -\sin\frac{\theta_\alpha}{2} \end{pmatrix}. \tag{33}$$

In this basis, intervalley matrix elements become

$$\langle K'\beta|\mathcal{P}_A\tau_-|K\alpha\rangle = e^{-i\phi_\beta}\cos^2\frac{\theta}{2},$$

$$\langle K\beta'|\mathcal{P}_A\tau_+|K'\alpha'\rangle = e^{i\phi_{\alpha'}}\cos^2\frac{\theta}{2},$$

$$\langle K'\beta|\mathcal{P}_B\tau_-|K\alpha\rangle = -e^{i\phi_\beta}\sin^2\frac{\theta}{2},$$

$$\langle K\beta'|\mathcal{P}_B\tau_+|K'\alpha'\rangle = -e^{-i\phi_{\alpha'}}\sin^2\frac{\theta}{2}. \tag{34}$$

Notice that their contribution to the scattering time is identical to Eq. (24). One finds, therefore, substituting Eqs. (20) and (34) into Eq. (25), that the scattering time becomes this time,

$$\frac{1}{\tau_K} = 4\pi\nu(E)\left(n_A u_A^2\cos^4\frac{\theta}{2} + n_B u_B^2\sin^4\frac{\theta}{2}\right)$$
$$= 2\eta_S\left(\cos^4\frac{\theta}{2} + \sin^4\frac{\theta}{2}\right) \equiv \frac{1}{\tau_S'}. \tag{35}$$

One can also verify that $1/\tau_{K'} = 1/\tau_K$. On the other hand, the expressions for $\gamma_{c,t}$ become also

$$\gamma_{c,t} = \pm e^{i(\phi_\alpha - \phi_\beta)}\left[n_A u_A^2\cos^4\frac{\theta}{2} + n_B u_B^2\sin^4\frac{\theta}{2}\right]$$
$$= \pm e^{i(\phi_\alpha - \phi_\beta)} \times n u_S^2\left[\cos^4\frac{\theta}{2} + \sin^4\frac{\theta}{2}\right]. \tag{36}$$

Notice that Eqs. (28) and (29) are always valid, whereas here $\Pi \simeq \tau_S'(1-\tau_S' Dq^2)$. Equations (35) and (36) suggest that in contrast to the topological mass case, the scattering time (the self-energy) and the bare vertex function (times Π) always cancel identically (giving unity) at the leading order of Eq. (29). As a consequence, the Cooperon diagram shows $1/q^2$ singularity, which occurs always at the $l=1$ channel,

$$\Gamma_t = \frac{-e^{i(\phi_\alpha - \phi_\beta)}}{2\tau_S'^2 Dq^2}, \tag{37}$$

where Γ_t is indeed *positive and singular, independent of* θ, indicating weak localization whenever the Fermi level is above the gap.

We have thus seen a clear distinction between two types of mass terms in their weak localization properties, as K-K' scattering is switched on. In the ordinary mass case, the system shows the orthogonal behavior, in sharp contrast to the unitary behavior of topological mass case. Such different weak localization properties due to different types of mass terms can be understood as follows. Recall that the topological mass term induces a finite σ_{xy}, if one picks up only one of the two real spin components. That was a clear signature of broken TRS, leading to unitary behavior. In the ordinary mass, on the other hand, contributions to σ_{xy} from each valley cancel, i.e., $\sigma_{xy}^K + \sigma_{xy}^{K'} = 0$. Therefore, there remains no trace of broken TRS any more, once two valleys are coupled by K-K' scattering. The ordinary mass term does preserve TRS, and as a result one finds always a diffusion-type $1/q^2$ singularity, leading to a weak localization behavior.

IV. RASHBA SPIN-ORBIT INTERACTION

Rashba spin-orbit interaction H_R is also an important factor for characterizing the physical properties of the doped Kane-Mele model. A finite Rashba term appears only when the system loses its inversion symmetry along the z axis (perpendicular to the 2D "graphene layer"). Physically, such breaking of inversion symmetry can be introduced by an asymmetric potential, e.g., when a graphene sheet is placed on a substrate. If Rashba spin-orbit interaction is stronger than a critical value ($\lambda_R > 2\Delta$), the system actually has no topologically nontrivial phase.[3] Here we suppose that Rashba spin-orbit interaction is not too strong and the undoped system is still in the topologically nontrivial phase. However, we show, in this section, that in regard to weak localization properties of our doped system, Rashba spin-orbit interaction is still a relevant perturbation and changes the symmetry class of our system as soon as it is turned on (in real samples of finite size of order L^2, there will be a crossover at the strength of Rashba spin-orbit interaction of order $\lambda_R \sim 1/L$). This is because the Rashba spin-orbit interaction mixes real spin up and down. Before switching on $\lambda_R \neq 0$, we did have real spin up and down but they were just there and inactive.

In the presence of H_R, we can still work on a 4×4-(instead of 8×8-)matrix space associated with $\vec{\sigma}$ and $\vec{s}$ since τ_z is diagonal in our basis. Focusing on one of the two valleys, say, K, one notices that the Rashba spin-orbit interaction couples A$\downarrow$ and B$\uparrow$ only (here, the up and down arrows refer to the real spin). The total Hamiltonian in the K valley reads

$$H_K = \begin{pmatrix} -\Delta & p_x - ip_y & 0 & 0 \\ p_x + ip_y & \Delta & i\lambda_R & 0 \\ 0 & -i\lambda_R & \Delta & p_x - ip_y \\ 0 & 0 & p_x + ip_y & -\Delta \end{pmatrix}, \tag{38}$$

where the inner 2×2 structure refers to AB spin, whereas the outer 2×2 block structure is associated with the real spin. Here, for the sake of simplicity, we consider only the case of Kane-Mele-type topological mass term: $\Delta\sigma_z\tau_z s_z$. After diagonalization, the resulting four energy bands are classified into two conduction and two valence bands, which we will call,

respectively, $u\pm$ and $d\pm$. The two valence bands $E_{d\pm}$ are degenerate on their top: the top position is always at $E=-\Delta$, unaffected by the Rashba term, whereas the conduction bands $E_{u\pm}$ are split by $2\lambda_R$,

$$E_{u\pm} = |\vec{p}_\pm| \pm \lambda_R/2 = \sqrt{p_x^2 + p_y^2 + (\Delta \pm \lambda_R/2)^2} \pm \lambda_R/2,$$

$$E_{d\pm} = -|\vec{p}_\pm| \pm \lambda_R/2 = -\sqrt{p_x^2 + p_y^2 + (\Delta \pm \lambda_R/2)^2} \pm \lambda_R/2. \tag{39}$$

The corresponding eigenvectors $|u\pm\rangle$ and $|d\pm\rangle$ can be conveniently parametrized by introducing a fictitious 3D momentum

$$\vec{p}_\pm = \begin{pmatrix} p_x \\ p_y \\ \Delta \pm \lambda_R/2 \end{pmatrix} \tag{40}$$

and associated polar angles

$$\cos\theta_\pm = \frac{\Delta \pm \lambda_R/2}{\sqrt{p_x^2 + p_y^2 + (\Delta \pm \lambda_R/2)^2}},$$

$$\cos\phi = \frac{p_x}{\sqrt{p_x^2 + p_y^2}}. \tag{41}$$

Note that ϕ is actually common to all cases. Thanks to the parameters introduced in Eq. (41), the eigenvectors corresponding to the eigenvalue $E_{u,d\pm}$, given in Eq. (39) allow for the following compact representation:

$$|Ku\pm\rangle = \frac{1}{\sqrt{2}} \begin{pmatrix} e^{-i\phi}\sin\frac{\theta_\pm}{2} \\ \cos\frac{\theta_\pm}{2} \\ \mp i\cos\frac{\theta_\pm}{2} \\ \mp ie^{i\phi}\sin\frac{\theta_\pm}{2} \end{pmatrix},$$

$$|Kd\pm\rangle = \frac{1}{\sqrt{2}} \begin{pmatrix} e^{-i\phi}\cos\frac{\theta_\pm}{2} \\ -\sin\frac{\theta_\pm}{2} \\ \pm i\sin\frac{\theta_\pm}{2} \\ \mp ie^{i\phi}\cos\frac{\theta_\pm}{2} \end{pmatrix}. \tag{42}$$

Note that a crucial difference here compared with the unitary limit ($\lambda_R=0$) is that because of the Rashba coupling, we have a stronger constraint on the choice of our basis and as a results there is no Berry phase in the matrix elements (see below). In the following, we consider again a doped system (our Fermi level is in the conduction band), i.e., $E>\Delta-\lambda_R$.

A. Long-range scatterers: Weak localization

The long-range scattering impurities do not couple K and K' valleys, and in a given valley do not distinguish A and B sites, i.e., its scattering potential is proportional to unity (no projection). In the following we focus on the K valley.

1. $\Delta-\lambda_R<E<\Delta+\lambda_R$ case

Let us first consider the case in which the Fermi level is close to the bottom of the conduction band, $\Delta-\lambda_R<E<\Delta+\lambda_R$. In this case only $|u-\rangle$ branch contributes to our diagrams. With this remark, we will omit, in the following, the indices u and $-$, for specifying a ket such as $|Ku-\alpha\rangle$, and denote it simply as $|K\alpha\rangle$. As we have seen in Eq. (42) because of the Rashba coupling, we have now a stronger constraint on the choice of our basis and as a results there is no Berry phase in the matrix element,

$$\langle K\beta|1\otimes 1|K\alpha\rangle = \cos(\phi_\alpha - \phi_\beta)\sin^2\frac{\theta_-}{2} + \cos^2\frac{\theta_-}{2}, \tag{43}$$

which is indeed *real*. Note that $|K\alpha\rangle$ here denotes $|Ku-\rangle$, given in Eq. (42), for a fictitious 3D momentum $\vec{p}_-$, given in Eq. (40), and specified by α. Self-energy diagrams give the bare scattering time (without vertex correction) as

$$\frac{1}{\tau_L} = \eta_L\left[\frac{1}{2}\sin^4\frac{\theta_-}{2} + \cos^4\frac{\theta_-}{2}\right]. \tag{44}$$

Because of the $\cos(\phi_\alpha-\phi_\beta)$ term in Eq. (43) the bare (and also dressed) vertex function has several angular momentum components. Naturally, we expand them such that

$$\gamma_{\alpha\beta} = \sum_l \gamma^{(l)}_{\alpha\beta} e^{il(\phi_\alpha-\phi_\beta)},$$

$$\Gamma_{\alpha\beta} = \sum_l \Gamma^{(l)}_{\alpha\beta} e^{il(\phi_\alpha-\phi_\beta)}. \tag{45}$$

The bare γ_l's are given as

$$\gamma^{(0)} = \eta_L\left[\frac{1}{2}\cos^4\frac{\theta_-}{2} + \sin^4\frac{\theta_-}{2}\right],$$

$$\gamma^{(1)} = \gamma^{(-1)} = \frac{\eta_L}{4}\cos^2\theta_-,$$

$$\gamma^{(2)} = \gamma^{(-2)} = \frac{\eta_L}{4}\sin^4\frac{\theta_-}{2}. \tag{46}$$

To solve the Bethe-Salpeter equations, first recall that there is an angular integration over the intermediate angle ϕ_μ, which forbids coupling between $\Gamma^{(l)}$'s with different angular momentum l. The Bethe-Salpeter equations take the form of Eq. (14). Then, comparing Eqs. (44) and (46), one can verify that Γ_0 shows a diffusion-type $1/q^2$ singularity, with a positive amplitude, leading to weak localization.

Recall that in the absence of Rashba spin-orbit interaction, the antilocalization tendency toward the graphene limit was given by the $l=1$ term. We emphasize that here the relevant (singular) contribution is from the $l=0$ channel and

this is quite contrasting to the former case (See Table IIin Sec. V). We mentioned earlier that as Rashba spin-orbit interaction $\lambda_R \neq 0$, with off-diagonal matrix elements in the real spin space, is turned on, the Berry phase, associated with the $1/q^2$ singularity of the $l=1$ channel, disappears. What we have discovered above is consistent with this observation. It is quite natural (as far as K' valley is switched off) that the $1/q^2$ singularity appearing in the $l=$(even) channel leads to weak localization, whereas in the $l=$(odd) case, the same singularity leads to weak antilocalization. From a perspective point of view, it is also useful to remark that the number N_s of effective spin degrees of freedom activated in the system is increased from $N_s=1$ ($\lambda_R=0$) to $N_s=2$ $\lambda_R \neq 0$, in switching on the Rashba term. This aspect will be more extensively discussed in Sec. V. The parity of N_s is a decisive factor for determining the symmetry class of system.

2. $\Delta+\lambda_R<E$ case

When the Fermi level is above the bottom of upper branch of the conduction band, i.e., when $\Delta+\lambda_R<E$, both $|Ku-\rangle$ and $|Ku+\rangle$ channels contribute to the weak localization properties. In order to shorten the equations, we omit in this section even the index K in the brackets and keep only $\pm$ for specifying branches, e.g., $|-\alpha\rangle \equiv |Ku-\alpha\rangle$. In this new notation,

$$\langle -\beta|1|-\alpha\rangle = \cos(\phi_\alpha - \phi_\beta)\sin^2\frac{\theta_-}{2} + \cos^2\frac{\theta_-}{2},$$

$$\langle +\beta|1|-\alpha\rangle = -i\sin(\phi_\alpha - \phi_\beta)\sin\frac{\theta_+}{2}\sin\frac{\theta_-}{2} = \langle -\beta|1|+\alpha\rangle,$$

$$\langle +\beta|1|+\alpha\rangle = \cos(\phi_\alpha - \phi_\beta)\sin^2\frac{\theta_+}{2} + \cos^2\frac{\theta_+}{2}. \quad (47)$$

Using these matrix elements, one can calculate the scattering time $\tau_\pm$ for the $|Ku\pm\rangle$ branch

$$\frac{1}{\tau_\pm} = \eta_L\left[\frac{1}{2}\sin^4\frac{\theta_\pm}{2} + \cos^4\frac{\theta_\pm}{2} + \frac{1}{2}\sin^2\frac{\theta_-}{2}\sin^2\frac{\theta_+}{2}\right], \quad (48)$$

where the last term corresponds to the contribution from interbranch matrix element, $|\langle +\beta|1|-\alpha\rangle|^2$.

The interbranch matrix elements in Eq. (47) also appear in the particle-particle ladders (see Figs. 4 and 5). In principle, the four electron states α, β, α', and β' can belong to either of the two channels, $|Ku-\rangle$ and $|Ku+\rangle$. There is, however, an important simplification at this level. Since we are interested only in the $1/q^2$ singular part of Cooperon diagrams, we need $p_\alpha + p_{\alpha'} = q \simeq 0$ and similarly, $p_\beta + p_{\beta'} = q \simeq 0$. This means that α and α' must belong to the same branch, which is similarly the case for β and β'. We are thus led to consider such diagrams as, γ_{--}, γ_{++}, γ_{-+}, and γ_{+-}. γ_{--} has already appeared in the regime, $\Delta-\lambda_R<E<\Delta+\lambda_R$ (its explicit form is also shown there in the form of expansion with respect to l). γ_{-+} is defined in Fig. 4(a). γ_{+-} is similar to γ_{-+}, only with $|Ku-\rangle$ and $|Ku+\rangle$ interchanged. Other γ's such as Figs. 4(b) and 4(c) are irrelevant to $1/q^2$ singularity. Explicit form of γ's are given as

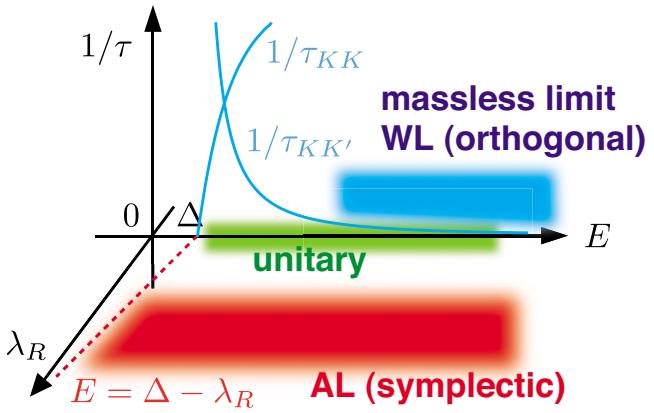

FIG. 4. (Color online) Topological mass case. Weak localization properties in the presence of short-range scatterers: intervalley scattering is allowed (K-K' coupled).

$$\gamma_{--} = \eta_L\left[\cos^2(\phi_\alpha - \phi_\beta)\sin^4\frac{\theta_-}{2} + 2\cos^2(\phi_\alpha - \phi_\beta)\sin^2\frac{\theta_-}{2}\cos^2\frac{\theta_-}{2} + \cos^4\frac{\theta_-}{2}\right],$$

$$\gamma_{++} = \eta_L\left[\cos^2(\phi_\alpha - \phi_\beta)\sin^4\frac{\theta_+}{2} + 2\cos^2(\phi_\alpha - \phi_\beta)\sin^2\frac{\theta_+}{2}\cos^2\frac{\theta_+}{2} + \cos^4\frac{\theta_+}{2}\right],$$

$$\gamma_{-+} = -\eta_L\sin^2(\phi_\alpha - \phi_\beta)\sin\frac{\theta_+}{2}\sin\frac{\theta_-}{2},$$

$$\gamma_{+-} = \gamma_{-+}. \quad (49)$$

The dressed Cooperon diagrams, Γ_{--} and Γ_{+-}, satisfy a coupled Bethe-Salpeter equation, which takes the following form:

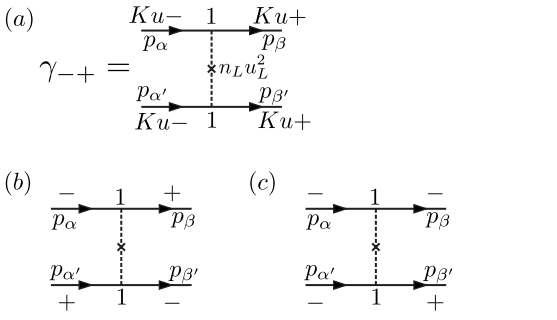

FIG. 5. Particle-particle ladders involving *interbranch* processes. In the presence of finite Rashba term $\lambda_R \neq 0$ (a) γ_{-+} does contributes to $1/q^2$ singularity, whereas such diagrams as (b) and (c) are irrelevant to the singularity since $p_\alpha + p_{\alpha'}$ cannot be smaller than the order of λ_R.

$$\begin{pmatrix}\Gamma_{--}\\ \Gamma_{+-}\end{pmatrix}=\begin{pmatrix}\gamma_{--}\\ \gamma_{+-}\end{pmatrix}+\begin{pmatrix}\gamma_{--}\Pi_{-} & \gamma_{-+}\Pi_{+}\\ \gamma_{+-}\Pi_{-} & \gamma_{++}\Pi_{+}\end{pmatrix}\begin{pmatrix}\Gamma_{--}\\ \Gamma_{+-}\end{pmatrix}, \tag{50}$$

where $\Pi_{\pm}\simeq\tau_{\pm}(1-D_{\pm}\tau_{\pm}q^2)$. Recall that in the last term of Eq. (50), combinations of the type, $\gamma\Pi\Gamma$, appear, which implicitly contain averages over the ϕ angle. We, therefore, expand bare γ's and dressed Γ's into different angular momentum contributions, as Eq. (45), and, to identify the singular contribution, pick up only the $l=0$ component. One way to convince oneself that the dressed Cooperons show indeed $1/q^2$ singularity at the $l=0$ channel is to prove the following identity:

$$\det\begin{pmatrix}1-\gamma_{--}^{(0)}\tau_{-} & -\gamma_{-+}^{(0)}\tau_{+}\\ -\gamma_{+-}^{(0)}\tau_{-} & 1-\gamma_{++}^{(0)}\tau_{+}\end{pmatrix}=0. \tag{51}$$

In order to verify, first notice

$$\gamma_{--}^{(0)}=\eta_L\left[\frac{1}{2}\cos^4\frac{\theta_{-}}{2}+\sin^4\frac{\theta_{-}}{2}\right],$$

$$\gamma_{-+}^{(0)}=-\frac{\eta_L}{2}\sin^2\frac{\theta_{-}}{2}\sin^2\frac{\theta_{+}}{2}=\gamma_{+-}^{(0)},$$

$$\gamma_{++}^{(0)}=\eta_L\left[\frac{1}{2}\cos^4\frac{\theta_{+}}{2}+\sin^4\frac{\theta_{+}}{2}\right] \tag{52}$$

and use such relations as

$$1-\gamma_{--}^{(0)}\tau_{-}=(1/\tau_{-}-\gamma_{--}^{(0)})\tau_{-}=\tau_{-}\frac{\eta_L}{2}\sin^2\frac{\theta_{+}}{2}\sin^2\frac{\theta_{-}}{2}=-\tau_{-}\gamma_{+-}^{(0)},$$

$$1-\gamma_{++}^{(0)}\tau_{+}=-\tau_{+}\gamma_{-+}^{(0)}. \tag{53}$$

Based on these observations, we claim that Rashba spin-orbit interaction recovers the $1/q^2$ singularity of Cooperons, driving the system back to weak localization (orthogonal symmetry class), whenever the Fermi level is above the gap. These features are illustrated in Fig. 1.

Let us finally consider what happens if one adiabatically switches off the Rashba term. The simplification we have made for justifying Eq. (50) is no longer valid. In the limit of vanishing λ_R we cannot simply neglect such diagrams as Figs. 4(b) and 4(c) and similar diagrams. In principle, they could contribute equally to the $1/q^2$ singularity if the singularity ever appears. Relations such as $p_\alpha+p_{\alpha'}=q\simeq 0$ can become satisfied in these diagrams. At the same time, inclusion of all such diagrams makes the size of coupled Bethe-Salpeter equation much bigger. One can no longer decouple Γ_{--} and Γ_{+-} as Eq. (50). The Cooperons acquire more channels to couple to, and as a result, the cancellation property between particle-particle ladders and the self-energy, such as Eq. (51), is lost. This loss of cancellation property due to activation of those channels which are depicted in Figs. 4(b) and 4(c) explains why the system becomes unitary in the $\lambda_R=0$ limit.

On the other hand, it is also possible to choose a basis if $\lambda_R=0$, as we did in Sec. III, in such a way that two upper band branches are decoupled. Recall that in the absence of Rashba term, the real spin part of the Hamiltonian is diagonalized in the real spin basis (by diagonalizing s_z).

B. Short-range scatterers: Weak antilocalization

In the presence of Rashba spin-orbit interaction, we found weak localization behavior for long-range scatterers, on contrary to the graphene limit (compare the first (i) and third (iii) row of Table III, left column). Note also that K-K' scattering drives the system, in the graphene limit, from symplectic to orthogonal symmetry class. We thus finally consider short-range scatterers in the presence of Rashba interaction. Since short-range scatterers involve intervalley scattering, we need to consider also the eigenstates at the K' valley. Diagonalizing the Hamiltonian at the K' valley, one verifies that the energy spectrum is identical to Eq. (39); there are two valence bands degenerate on their top at $E=-\Delta$, whereas two conduction bands split by $2\lambda_R$. Using the same parameterization as before, i.e., Eqs. (40) and (41), the corresponding eigenvectors read

$$|K'u\pm\rangle=\frac{1}{\sqrt{2}}\begin{pmatrix}\cos\frac{\theta_{\pm}}{2}\\ -e^{-i\phi}\sin\frac{\theta_{\pm}}{2}\\ \mp ie^{i\phi}\sin\frac{\theta_{\pm}}{2}\\ \pm i\cos\frac{\theta_{\pm}}{2}\end{pmatrix},$$

$$|K'd\pm\rangle=\frac{1}{\sqrt{2}}\begin{pmatrix}\sin\frac{\theta_{-}}{2}\\ e^{-i\phi}\cos\frac{\theta_{-}}{2}\\ \pm ie^{i\phi}\cos\frac{\theta_{-}}{2}\\ \pm i\sin\frac{\theta_{-}}{2}\end{pmatrix}. \tag{54}$$

Short-range scatterers do distinguish AB pseudospin, whereas as far as they are nonmagnetic impurities, they are unconcerned about the real spin. The impurity potential operator is proportional to $\mathcal{P}_{A,B}$, which should be understood here as

$$\mathcal{P}_{A,B}\otimes 1=\begin{pmatrix}\mathcal{P}_{A,B} & 0\\ 0 & \mathcal{P}_{A,B}\end{pmatrix}. \tag{55}$$

Let us focus on the regime: $\Delta-\lambda_R<E<\Delta+\lambda_R$ in which only $|Ku-\rangle$ and $|K'u-\rangle$ modes are available. Using $\alpha,\beta,\ldots$ for specifying momenta, the relevant matrix elements read

$$\langle K'\beta|\mathcal{P}_A\tau_{-}|K\alpha\rangle=\frac{e^{-i\phi_\beta}+e^{-i\phi_\alpha}}{4}\sin\theta_{-},$$

$$\langle K\beta'|\mathcal{P}_A\tau_+|K'\alpha'\rangle = \frac{e^{i\phi_{\beta'}}+e^{i\phi_{\alpha'}}}{4}\sin\theta_- \simeq -\frac{e^{i\phi_\beta}+e^{i\phi_\alpha}}{4}\sin\theta_-. \tag{56}$$

As for the latter matrix element, we noticed $\phi_{\alpha'} \simeq \phi_\alpha + \pi$ and $\phi_{\beta'} \simeq \phi_\beta + \pi$ in the second expression. This clarifies the nature of additional minus sign analogous to Eq. (30). As for particle-particle ladders, they are, as before, classified into KK, KK'-mixed, and $K'K'$ sectors. We focus again on the $J=0$ sector in which two types of bare vertex functions, $\gamma_\pm$, are possible, and correspondingly, two types of Cooperons: $\Gamma_\pm$ (recall Fig. 2). $\Gamma_\pm$ obeys a coupled Bethe-Salpeter equation, Eq. (50). Again, as a result of projection $\mathcal{P}_A, \mathcal{P}_B$ and K-K' scattering, γ_t acquires an additional minus sign

$$\gamma_t = -\frac{\eta_S}{4}\cos^2\frac{\phi_\alpha - \phi_\beta}{2}\sin^2\theta_-. \tag{57}$$

However, in the present case, the Berry phase had disappeared, implying that this time the new minus sign leads the system from orthogonal to symplectic. To verify this, first notice that intravalley matrix elements are given as

$$\langle K\beta|\mathcal{P}_A|K\alpha\rangle = \frac{1}{2}\left[e^{-i(\phi_\alpha-\phi_\beta)}\sin^2\frac{\theta_-}{2} + \cos^2\frac{\theta_-}{2}\right],$$

$$\langle K'\beta|\mathcal{P}_A|K'\alpha\rangle = \frac{1}{2}\left[\cos^2\frac{\theta_-}{2} + e^{i(\phi_\alpha-\phi_\beta)}\sin^2\frac{\theta_-}{2}\right]. \tag{58}$$

These combine to give

$$\gamma_c = \frac{\eta_S}{4}\left[\cos^4\frac{\theta_-}{2} + \cos(\phi_\alpha-\phi_\beta)\frac{\sin^2\theta_-}{2} + \sin^4\frac{\theta_-}{2}\right], \tag{59}$$

which is indeed positive. The scattering time is also calculated to be

$$1/\tau_K = 1/\tau_{K'} = \eta_S/4. \tag{60}$$

Note that all θ_- dependence cancelled, giving unity.

Let us now sum up the particle-particle ladders and then solve Bethe-Salpeter equation. After diagonalization, one finds

$$\Gamma_c + \Gamma_t \sim (\text{regular}),$$

$$[1-(\gamma_c-\gamma_t)\Pi](\Gamma_c-\Gamma_t) = \gamma_c - \gamma_t > 0. \tag{61}$$

In order to identify the singular contribution, one should expand γ's and Γ's into different angular momentum components, and pick up the $l=0$ term. Other contributions are indeed regular. Comparing Eqs. (57), (59), and (60), one can indeed verify that $\Gamma_c - \Gamma_t$ shows $1/q^2$ singularity, whereas only Γ_t contributes to the conductivity, giving weak antilocalization correction.

Based on this observation, together with our analysis in the long-range case for the regime: $E > \Delta + \lambda_R$, one can naturally conjecture that this symplectic tendency continues to the higher energy regime: $E > \Delta + \lambda_R$. Then, the phase diagram in the presence of K-K' scattering (Fig. 3) becomes predominantly symplectic (when $\lambda_R \neq 0$). Comparing two phase diagrams, in the absence (Fig. 1) and presence (Fig. 3) of K-K' scattering, one can see that the two weak antilocalization behaviors, one in the graphene limit and the other of Z_2 topological insulator phase, have a quite different origin. The former occurs in a single Dirac cone, whereas the latter occurs due to K-K' scattering. The former is related to Berry phase à la Ref. 42, whereas in the presence of Rashba term mixing real spins, the matrix elements become real (the Berry phase disappears).

Let us finally estimate the strength of gate electric field required for observing the crossover to weak antilocalization. For the crossover to be experimentally accessible, Rashba SOI needs to be the order of ~ 1 K. This corresponds to the electric field of order ~ 1 V/nm[5], a value attainable in double-gated graphene devices.[47] The crossover to weak antilocalization will be observed for a sample with insignificant ripples. A similar crossover due to Rashba SOI has been observed in another context in InGaAs/InAlAs quantum well.[48]

V. SUMMARY AND DISCUSSIONS

We have studied localization properties of the doped Kane-Mele model. We assumed that the disorder is weak enough to apply the standard weak localization theory, i.e., we have focused on the leading order $1/g$ correction in the $1/g$ expansion of $\beta(g)$. We have considered a phase diagram in the (E, λ_R) plane together with inverse lifetime of a Cooperon, $1/\tau$, in order to indicate the crossover behavior in the unitary case. When $\tau \to \infty$, the corresponding Cooperon mode shows $1/q^2$ singularity and gives correction to the β function. Otherwise there is no correction to the β function at the $1/g$ level and in the $L \to \infty$ limit. In the presence of topological mass term, the system shows predominantly a unitary behavior, as expected from symmetry consideration. However, as we have seen in Secs. III and IV, the role of mass term to system's localization property is a more subtle issue, depending on the type of impurities and the presence or absence of Rashba spin-orbit interaction.

A broader perspective is obtained on the phase diagram of localization properties in terms of the number N_s of *activated* (pseudo) spin degrees of freedom. Table II summarizes the WL properties of doped Kane-Mele model. It shows that contrasting behaviors are closely related to the *parity* of N_s. If a mass term is negligible and if N_s is even, the system shows WL, whereas if N_s is odd, the system undergoes weak antilocalization (AL). The unitary behavior, on the other hand, is independent of the parity of N_s and emerges whenever the effective time-reversal symmetry, i.e., TRS or PTRS, is broken (see Table III). Thus, in order to identify the weak localization symmetry class, it is most important to count active spin degrees of freedom, and whether the effective time-reversal symmetry is preserved. Note that the pseudospin $\vec{\sigma}$ is odd under pseudo TRS but even under the genuine TRS. Therefore the ordinary mass term in the third column does not break the TRS and the case (a) shows the orthogonal behavior.

In order to distinguish active and inactive spins, we introduce TRS operation, T_Σ, defined in the subspace Σ, of acti-

TABLE II. Summary: weak localization properties of the Kane-Mele model. The WL or weak AL results depending on the presence or absence of intervalley scattering and Rashba spin-orbit interaction. Notice the role of N_s, the number of activated (pseudo) spin species. The value of angular momentum l is also indicated for the singular ($\sim 1/q^2$) Cooperon channel [see Eq. (45)]. In the presence of K-K' scattering, activation of the valley spin increases N_s by one, leading to change in weak localization properties.

	Long-range scatterers (no K-K' scattering)	Short-range scatterers (K and K' points coupled)
(i) Ideal massless graphene	$\vec{\sigma}$: $N_s=1$ (odd) $1/q^2$: $l=1\rightarrow$AL	$\vec{\sigma}$, $\vec{\tau}$: $N_s=2$ (even) $1/q^2$: $l=1\rightarrow$WL
(ii) Gapped cases (a) topological mass (b) ordinary mass	$\vec{\sigma}$: $N_s=1$ (odd) unitary (WAL as $E\rightarrow\infty$)	$\vec{\sigma}$, $\vec{\tau}$: $N_s=2$ (even) (a) unitary (WL as $E\rightarrow\infty$) (b) $1/q^2$: $l=1\rightarrow$ WL
(iii) doped Z_2 insulator	$\vec{\sigma}$, $\vec{s}$: $N_s=2$ (even) $1/q^2$: $l=0\rightarrow$ WL	$\vec{\sigma}$, $\vec{\tau}$,$\vec{s}$: $N_s=3$ (odd) $1/q^2$: $l=0\rightarrow$ AL

vated spins, where $\Sigma=\{\vec{\sigma}\}$, $\{\vec{\sigma},\vec{\tau}\}$, $\{\vec{\sigma},\vec{s}\}$, and $\{\vec{\sigma},\vec{\tau},\vec{s}\}$. Note that when some of the effective spin degrees of freedom are inactive, the total Hamiltonian including the scattering potential becomes block diagonal, since it has no off-diagonal components in the space of inactivated spins. The relevant TRS operation T_Σ *leaves each of such blocks invariant*. The relevant TRS operations are given explicitly as,

$$T_\sigma = -i\sigma_y C, \quad T_{\sigma\tau} = \tau_x C,$$

$$T_{\sigma s} = (-i\sigma_y)(-is_y)C, \quad T_{\sigma\tau s} = \tau_x(-is_y)C, \tag{62}$$

where C is complex conjugation. $T_{\sigma\tau s}$ represents the genuine TRS operation. Effective TRS of the system is, therefore, determined by the transformation property of the mass term under T_Σ (see Table III). When a mass term is odd against TRS, the system shows the unitary behavior. If some (pseudo or genuine) TRS exists in the system, its weak localization property is determined by the number N_s of the activated spin degrees of freedom. One can verify $T_\Sigma^2=1$ if N_s is even, whereas $T_\Sigma^2=-1$ if N_s is odd. The former (latter) corresponds to the orthogonal (symplectic) class in the random matrix theory[28] and leads to constructive (destructive) interference between two scattering processes transformed from one to the other by T_Σ.

The above symmetry arguments allow for a slight generalization of our localization phase diagram (see Fig. 1). Recall that in Sec. IV A, we have chosen the mass to be $H_2=-\Delta\sigma_z s_z$. Results of this analysis are consistent with the symmetry consideration. In Fig. 1, we further conjecture based on the symmetry consideration that a similar analysis for an ionic mass term $H_2=M\sigma_z$ leads to the absence of WL (unitary behavior). Thus, the four minus signs in Table III correspond to four unitary phases in Fig. 1. We also point out that in terms of symmetry, ripples play the same role as the ionic mass.

We mention that the results of our analyses summarized in Table II and Fig. 1 are also relevant to *intrinsic* single-valley systems,[4] such as the one realized in HgTe/CdTe quantum well.[8] In the latter system, a single pair (Kramers pair) of Dirac cones appear, in contrast to graphene (cf. graphene has two pairs of Dirac cones; they appear at K and K' points). Note that two Dirac cones (Kramers pair with real spin $\uparrow$ and $\downarrow$), described in the model introduced in Ref. 4, have the *same* sign for their mass term, implying (superficially) the ordinary (ionic) mass case in our language. However, they have also different chiralities and by a simple linear transformation (exchange of rows and columns), they can be mapped, and indeed corresponds to the topological mass case, studied in Sec. IV A. Our diagnosis (see Table II and also Fig. 1) suggests that the single-valley HgTe/CdTe system shows a crossover from unitary to orthogonal (WL) symmetry class, on activating the real spin degrees of freedom by a (Rashba-type) off-diagonal interaction between real spin $\uparrow$ and $\downarrow$ sectors.

What is then essential to the AL behavior characteristic to the doped Kane-Mele model? As can be guessed by the analysis relying on the number N_s of active spin species, the combination of Rashba interaction and the K-K' scattering makes $N_s=3$. In other words, the AL results even in the absence of the topological mass term or even in the case of the ordinary mass term. In this sense, the AL is not a peculiar

TABLE III. (Pseudo) time-reversal operations T_Σ, relevant in the subspace spanned by activated spins. Transformation property of a mass term $\mathcal{O}=M\sigma_z,\Delta\sigma_z\tau_z s_z$ under T_Σ: $T_\Sigma \mathcal{O} T_\Sigma^{-1}=\pm\mathcal{O}$. The sign appears in the table. U refers to unitary class.

Activated spins	$\vec{\sigma}$	$\vec{\sigma},\vec{\tau}$	$\vec{\sigma},\vec{s}$	$\vec{\sigma},\vec{\tau},\vec{s}$
Relevant TRS operation	T_σ	$T_{\sigma\tau}$	$T_{\sigma s}$	$T_{\sigma\tau s}$
σ_z	$-\rightarrow U$	$+$	$-\rightarrow U$	$+$
$\Delta\sigma_z\tau_z s_z$	$-\rightarrow U$	$-\rightarrow U$	$+$	$+$

property of the doped Z_2 insulator. The hallmark of the doped Z_2 insulator becomes manifest in the absence of the Rashba interaction. Namely, the robustness of the unitary behavior against the range of the disorder potential is a fingerprint of topological mass term. The unitary behavior is closely related to the quantized spin-Hall effect in the undoped case.

Finally, we comment on the role of the channel index l which is a quantum number associated with a relative momentum of electrons before and after the scattering by an impurity. See Eqs. (11) and (45) for its definition. As we have already seen in the body of the paper, to identify the singular channel l greatly helps to determine the weak localization property. In the case of long-range scatterers, the two valleys are decoupled and we can safely focus on, say, the K valley. Then, in Secs. III and IV, we have seen that the $1/q^2$ singularity appearing in the $l=$(even) channel leads to WL, whereas in the $l=$(odd) case, the same singularity leads to AL, This situation is reversed in the presence of K-K' scattering: even l leads to AL and odd l to WL according to Table II.

The above selection rule on the singular channel l is superficially dependent on the choice of the spin part of the wave function. In Secs. II and III, we have chosen to use a single-valued two-component spinor for describing AB sublattice spin eigenstates, which were naturally extended to the single-valued four-component spinor in the presence of Rashba spin-orbit interaction. If one choose a double-valued spinor instead of Eq. (3), pretending that the AB-sublattice spin realizes a real spin, then the selection rule is shifted by one. This shift, however, is the same for all cases in Table II. Hence if we take the difference of l relative to the graphene limit, for example, the WL or AL behavior does not depend on the choice of the spin eigenstates.

As we have seen in Secs. III and IV, the value l of singular channel does not change in the presence of K-K' scattering, The value of N_s is, on the other hand, increased by one, in switching on the KK' valley-spin $\vec{\tau}$. Since $\vec{\tau}$ flip does not involve ϕ_α variables, the value l of the singular channel remains the same. However, the nature of the channel does change by the K-K' scattering. Namely, switching on of the valley spin appears as an additional minus sign in particle-particle ladders.

In conclusion, we have constructed a poor man's phase diagram of the doped and disordered Kane-Mele model. In order to characterize the Z_2 nature of the model, we considered a doped case in contrast to the more familiar topological insulator phase. We also characterized the Z_2 nature from its bulk properties, instead of its *edge* properties, to which the Z_2 nature is often attributed.[2,7] Our analysis is restricted to the weak (anti)localization level and can be used for constructing an effective σ-model description[31] of the same model. The basic mechanism discussed here will be also useful for the understanding of different types of topological insulators.

ACKNOWLEDGMENTS

K.I. and K.N. acknowledge support from KAKENHI Grant-in-Aid for Young Scientists (Grant Nos. 19740189 and 20740167.

[1] For research activities in graphene from a more general point of view, see, e.g., A. K. Geim and K. S. Novoselov, Nature Mater. **6**, 183 (2007), and references therein.
[2] C. L. Kane and E. J. Mele, Phys. Rev. Lett. **95**, 226801 (2005).
[3] C. L. Kane and E. J. Mele, Phys. Rev. Lett. **95**, 146802 (2005).
[4] B. A. Bernevig, T. L. Hughes, and S.-C. Zhang, Science **314**, 1757 (2006).
[5] H. Min, J. E. Hill, N. A. Sinitsyn, B. R. Sahu, L. Kleinman, and A. H. MacDonald, Phys. Rev. B **74**, 165310 (2006).
[6] D. Huertas-Hernando, F. Guinea, and A. Brataas, Phys. Rev. B **74**, 155426 (2006).
[7] Y. Yao, F. Ye, X. L. Qi, S. C. Zhang, Z. Fang, Phys. Rev. B **75**, 041401(R) (2007).
[8] M. König, S. Wiedmann, C. Brüne, A. Roth, H. Buhmann, L. W. Molenkamp, X.-L. Qi, and S.-C. Zhang, Science **318**, 766 (2007).
[9] M. Gmitra, S. Konschuh, C. Ertler, C. Ambrosch-Draxl, and J. Fabian, arXiv:0904.3315 (unpublished).
[10] L. Fu, C. L. Kane, and E. J. Mele, Phys. Rev. Lett. **98**, 106803 (2007); Phys. Rev. B **76**, 045302 (2007).
[11] S. Murakami, Phys. Rev. Lett. **97**, 236805 (2006).
[12] J. E. Moore and L. Balents, Phys. Rev. B **75**, 121306(R) (2007).
[13] X.-L. Qi, T. L. Hughes, and S.-C. Zhang, Phys. Rev. B **78**, 195424 (2008).
[14] A. P. Schnyder, S. Ryu, A. Furusaki, and A. W. W. Ludwig, Phys. Rev. B **78**, 195125 (2008).
[15] D. Hsieh, D. Qian, L. Wray, Y. Xia, Y. S. Hor, R. J. Cava, and M. Z. Hasan, Nature (London) **452**, 970 (2008).
[16] R. Shindou and S. Murakami, Phys. Rev. B **79**, 045321 (2009).
[17] D. Hsieh, Y. Xia, D. Qian, L. Wray, J. Dil, F. Meier, L. Patthey, J. Osterwalder, A. Fedorov, H. Lin, A. Bansil, D. Grauer, Y. Hor, R. Cava, and M. Hasan, arXiv:0904.1260 (unpublished).
[18] M. Onoda, Y. Avishai, and N. Nagaosa, Phys. Rev. Lett. **98**, 076802 (2007).
[19] H. Obuse, A. Furusaki, S. Ryu, and C. Mudry, Phys. Rev. B **76**, 075301 (2007); **78**, 115301 (2008).
[20] T. Nakanishi and T. Ando, J. Phys. Soc. Jpn. **68**, 561 (1999).
[21] K.-I. Imura, Y. Kuramoto, and K. Nomura, arXiv:0904.1676 (unpublished).
[22] The sign of topological mass is taken to be opposite to the original Kane-Mele paper (Ref. 2). This is only for later purpose of making phase diagrams more concise. Physically, the sign of Δ is determined by the the sign of next-nearest-neighbor imaginary hopping, which is irrelvant to the localization properties.
[23] H. Suzuura and T. Ando, Phys. Rev. Lett. **89**, 266603 (2002); E. McCann, K. Kechedzhi, V. I. Falko, H. Suzuura, T. Ando, and B. L. Altshuler, *ibid.* **97**, 146805 (2006).
[24] K. Nomura, M. Koshino, and S. Ryu, Phys. Rev. Lett. **99**,

146806 (2007).
[25] J. H. Bardarson, J. Tworzydlo, P. W. Brouwer, and C. W. J. Beenakker, Phys. Rev. Lett. **99**, 106801 (2007).
[26] A. Lherbier, B. Biel, Y. M. Niquet, and S. Roche, Phys. Rev. Lett. **100**, 036803 (2008).
[27] I. L. Aleiner and K. B. Efetov, Phys. Rev. Lett. **97**, 236801 (2006); A. Altland, *ibid.* **97**, 236802 (2006); D. V. Khveshchenko, *ibid.* **97**, 036802 (2006).
[28] F. J. Dyson, J. Math. Phys. **3**, 140 (1962).
[29] P. Fendley, Phys. Rev. B **63**, 104429 (2001); S. Ryu, C. Mudry, H. Obuse, and A. Furusaki, Phys. Rev. Lett. **99**, 116601 (2007).
[30] A. W. W. Ludwig, M. P. A. Fisher, R. Shankar, and G. Grinstein, Phys. Rev. B **50**, 7526 (1994).
[31] A. M. M. Pruisken, Nucl. Phys. B **235**, 277 (1984).
[32] G. W. Semenoff, Phys. Rev. Lett. **53**, 2449 (1984).
[33] F. D. M. Haldane, Phys. Rev. Lett. **61**, 2015 (1988).
[34] A. Bostwick, Taisuke Ohta, Thomas Seyller, Karsten Horn, and Eli Rotenberg, Nat. Phys. **3**, 36 (2007).
[35] S. Y. Zhou, G.-H. Gweon, A. V. Fedorov, P. N. First, W. A. de Heer, D.-H. Lee, F. Guinea, A. H. Castro Neto and A. Lanzara, Nature Mater. **6**, 770 (2007).
[36] S. V. Morozov, K. S. Novoselov, M. I. Katsnelson, F. Schedin, L. A. Ponomarenko, D. Jiang, and A. K. Geim, Phys. Rev. Lett. **97**, 016801 (2006); Y.-W. Tan, Y. Zhang, H. L. Stormer, and P. Kim, Eur. Phys. J. Spec. Top. **148**, 15 (2007).
[37] X. Wu, X. Li, Z. Song, C. Berger, and W. A. deHeer, Phys. Rev. Lett. **98**, 136801 (2007).
[38] F. V. Tikhonenko, D. W. Horsell, R. V. Gorbachev, and A. K. Savchenko, Phys. Rev. Lett. **100**, 056802 (2008).
[39] A. F. Morpurgo and F. Guinea, Phys. Rev. Lett. **97**, 196804 (2006).
[40] K. Nomura, S. Ryu, M. Koshino, C. Mudry, and A. Furusaki, Phys. Rev. Lett. **100**, 246806 (2008).
[41] M. V. Berry,Proc. R. Soc. London Ser. A **392**, 45 (1984).
[42] T. Ando, T. Nakanishi, and R. Saito, J. Phys. Soc. Jpn. **67**, 2857 (1998).
[43] See, e.g., S. Chakravarty and A. Schmid, Phys. Rep. **140**, 193 (1986); G. Bergman, *ibid.* **107**, 1 (1984), and references therein.
[44] S. Hikami, A. I. Larkin, and Y. Nagaoka, Prog. Theor. Phys. **63**, 707 (1980); S. Maekawa and H. Fukuyama, J. Phys. Soc. Jpn. **50**, 2516 (1981); H. Fukuyama, *ibid.* **51**, 1105 (1982).
[45] B. L. Altshuler, D. Khmelnitzkii, A. I. Larkin, and P. A. Lee, Phys. Rev. B **22**, 5142 (1980).
[46] A similar circumstance occurs in the conventional analysis of weak antilocalization à la Ref. 44. When one considers scattering due to spin-orbit coupling, $\vec{l}\cdot\vec{s}$-type isotropic term leads, as is well known, to weak antilocalization. On the contrary, if one keeps only $l_z s_z$ component, then the system is known to stay, in this case, orthogonal (in our case the system stays unitary when $\lambda_R=0$).
[47] J. B. Oostinga, Hubert B. Heersche, Xinglan Liu, Alberto F. Morpurgo, and Lieven M. K. Vandersypen, Nature Mater. **7**, 151 (2007).
[48] T. Koga, J. Nitta, T. Akazaki, and H. Takayanagi, Phys. Rev. Lett. **89**, 046801 (2002).